Ion Concentration of External Solution as a Characteristic of Micro- and Nanogel Ionic Reservoirs

ARTICLE *in* THE JOURNAL OF PHYSICAL CHEMISTRY B · SEPTEMBER 2006

Impact Factor: 3.3 · DOI: 10.1021/jp061044i · Source: PubMed

6 AUTHORS, INCLUDING:

Sergey Kazakov
Pace University
47 PUBLICATIONS **436** CITATIONS
SEE PROFILE

Irina G Gazaryan
Burke Medical Research Institute New York
89 PUBLICATIONS **2,347** CITATIONS
SEE PROFILE

Boris Krasnikov
New York Medical College
43 PUBLICATIONS **1,069** CITATIONS
SEE PROFILE

Kalle Levon
Polytechnic Institute of New York University
128 PUBLICATIONS **2,098** CITATIONS
SEE PROFILE

Ion Concentration of External Solution as a Characteristic of Micro- and Nanogel Ionic Reservoirs

Sergey Kazakov,*,† Marian Kaholek,‡ Irina Gazaryan,§ Boris Krasnikov,§ Korki Miller,† and Kalle Levon‡

Department of Chemistry and Physical Sciences, Pace University, 861 Bedford Road, Pleasantville, New York 10570, Polymer Research Institute, Polytechnic University, Six MetroTech Center, Brooklyn, New York 11201, and Burke Medical Research Institute, 785 Mamaroneck Avenue, White Plains, New York 10605

Received: February 17, 2006; In Final Form: June 12, 2006

Ion-sensitive hydrogel is regarded as an ionic reservoir, i.e., a system capable of changing the external pH or ionic strength by accumulating or releasing ions. The concept of a hydrogel ionic reservoir was demonstrated for hydrogel particles of three different size ranges: macrogel (1000−6000 μm), microgel (~20−200 μm), and nanogel (~0.2 μm). Ion sensitivity of poly(*N*-isopropylacrylamide-*co*-1-vinylimidazole) (PNIPA-VI) microgels with imidazolyl (ionizable) groups was confirmed by the pH dependence of their volume, while nanogels were characterized by dynamic light scattering. On the contrary, the volume of poly(*N*-isopropylacrylamide) (PNIPA) microgels without ionizable groups was pH independent in the whole range of pH from 10 to 2. Four distinct regions of pH-behavior were observed for PNIPA-VI hydrogel micro- and nanoparticles using potentiometric titration of their suspensions. Time-resolved measurements of ion concentrations in the suspension of hydrogel particles revealed a substantial difference in kinetics of pH equilibration for (i) ion-sensitive hydrogels (PNIPA-VI) vs hydrogels without ionizable groups (PNIPA) and (ii) PNIPA-VI hydrogels of different sizes. On the basis of the experimental observations, a two-step mechanism affecting the kinetics of proton uptake into the hydrogel particles with ionizable groups was proposed: (1) fast binding of ions to the immediate surface of each particle and (2) a slower successive diffusion of bound sites into the next inner layer of polymer network. In accord with the mechanism proposed, a quasi-chemical kinetic model of pH relaxation to equilibrium was developed to fit the experimental data for the time course of proton uptake by macro-, micro-, and nanogels into two exponentials with the characteristic times of τ_1 and τ_2. We believe the same kinetic model will be pertinent to describe phenomenological and molecular mechanisms controlling proton transport in/out bacteria, cells, organelles, drug delivery vehicles, and other natural or artificial multifunctional ionic containers. The approach can be easily extended for the other ions (e.g., Na^+, K^+, and Ca^{2+}).

Introduction

Ion-sensitive hydrogels are of great potential for diverse applications, such as an environmentally responsive element in drug delivery systems,[1,2] compliant actuators or "artificial muscles",[3−7] and an element supporting bilayer lipid membrane in biosensory devices.[8−10] According to the recognized concept of a gel-like cytoplasm,[11] a cytoplasmic protein−ion−water matrix may operate by the same working principles as an ordinary hydrogel ionic reservoir. Thus, the kinetics of ion exchange within the artificial polymer networks may model some of the living cell functions.

The physical dimension of polymer networks containing ionizable groups results from a balance between the electrostatic interactions of charged polymer chains and network elasticity,[12−27] i.e., the ability of ion-responsive hydrogels to swell or shrink reversibly is mainly controlled by the charge on the network, the counterions associated with the network charge, and the difference in concentration of mobile ions inside hydrogel and in the exterior solution. The ion-responsive polymer network is able to store intrinsic chemical energy by accumulating or releasing ions.[26,28]

The interior of an ionic hydrogel particle bearing many charged (ionizable) groups that cannot move out of the gel, may be considered as a solution separated from the external solution by a semipermeable membrane. The equilibrium distribution of ions between those hydrogel particles and external solution is determined by a Donnan theory. A vast pool of relatively recent studies [refs 18−26, 29−34, and references therein] has been devoted to the charge controlled behavior of ionic microgels in *equilibrium*. Our particular interest is in the transitional kinetics of approaching the ionic equilibrium in the hydrogel particles' suspensions, i.e., the time course of external pH changes when a hydrogel with the known concentration of ionizable groups is added to or when an acid or base is injected into the hydrogel suspension. Since the regulation of external pH and/or ion concentration produces electrochemical and mechanical transformations in the polymeric network, the rates of those responses are important quantitative characteristics of the ionic reservoir, though unknown. Nonetheless, one can assume that the rate and effectiveness of the ionic reservoir in accumulating or releasing ions can be increased by decreasing the size of hydrogel particles. This effect remains to be proven, however.

* To whom correspondence should be addressed. Phone: (914) 773-3774. Fax: (914) 773-3418. E-mail: skazakov@pace.edu.
† Pace University.
‡ Polytechnic University.
§ Burke Medical Research Institute.

10.1021/jp061044i CCC: $33.50
Published on Web 07/15/2006

In this work, we examine the pH-equilibration in the suspensions of hydrogel macro-, micro-, and nanoparticles containing *N*-isopropylacrylamide and 1-vinylimidazole (PNIPA-VI) by measuring proton concentration in the exterior to hydrogels. Our hypothesis is in that the charges fixed on the polymer network can affect the distribution of diffusible ions between the external solution and the gel interior. If there is an excess of ions in the external solution with respect to the gel interior, the ions diffuse inside and bind to the ionizable groups. If the concentration of ions in the external solution is less than that inside the gel, the ionizable groups within the gel release ions into the gel exterior. The number of ionizable groups on the cross-linked polymer chains defines the gel ionic capacity.

By measurement of the pH in the environment surrounding hydrogel particles of macro- and micrometer sizes, we attempt to reveal the kinetic mechanisms affecting proton uptake into the hydrogel particles with ionizable groups, i.e., the mechanism of pH equilibration in the polymer network interior. The issues of exchanging ions with surroundings are also addressed through (1) potentiometric titration of PNIPA-VI and PNIPA hydrogel particles and (2) comparison of the titration curves for the suspensions of PNIPA-VI hydrogel particles of different sizes. On the basis of the experimental observations, the quasichemical kinetic model is developed to describe pH equilibration after acid injection into the suspensions of hydrogel of different sizes. One can predict that the model may be universal in terms of applicability for different artificial and natural ionic reservoirs.

Experimental Section

Materials. *N*-Isopropylacrylamide (NIPA) and 1-vinylimidazole (VI) monomers and *N*,*N*′-methylenebisacrylamide (MBA) were purchased from Aldrich (Milwaukee, WI). Chloroform solution of L-α-phosphatidylcholine from egg yolk (EPC, transition temperature $T_m = -2$ °C, $M_w = 760$ g/mol) was purchased from Avanti Polar Lipids (Alabaster, AL). 2,2-Diethoxyacetophenone (DEAP) and nonionic detergent Triton X-100 (T_{X-100}) were purchased from Fluka (Milwaukee) and Eastman Kodak (Rochester), respectively. Chemicals were used directly without additional purification. Water was purified by Milli-Q (Millipore). Tris-HCl buffer (50 mM, pH 7.5) was used in the experiments. To adjust pH, 0.1 M HCl or 0.1 M NaOH was used.

Bulky Gel and Microgels Preparation. The method for preparation of chemically cross-linked hydrogel has been described elsewhere.[10,35] In brief, polymerization of a hydrogel-forming medium was induced by a Blak Ray UV-lamp (365 nm, 100 W) in the presence of a photoinitiator. The polymerization time was 2 h. Two types of hydrogels, ion-sensitive and ion-insensitive, were prepared. The hydrogel-forming solution for ion sensitive gel (PNIPA-VI) consisted of 5.5 wt % of NIPA, 2 wt % of VI, 0.5 wt % of MBA, and 0.1 wt % of DEAP. The hydrogel-forming solution for the ion-insensitive gel (PNIPA) consisted of 7.0 wt % of NIPA, 0.5 wt % of MBA, and 0.1 wt % of DEAP. The polymerization temperature (20 °C) was below the lower critical volume phase transition temperature both for PNIPA ($T_V \approx 32$ °C) and PNIPA-VI (37 °C). Thus prepared macrogels were washed with a large amount of distilled water so that the final pH of the hydrogels was equal to the pH of water 5.85. Macrogel with the size of a few millimeters was prepared by squeezing hydrogel through the ~2 mm syringe's pinhole.

Microgels were prepared by squeezing the same hydrogel as for macrogel in the syringe to remove water and then pressing through a metallic membrane with 160-μm pores. The obtained particles were suspended in water.

Optical Microscopy. Suspensions of macro- and microgels were observed either in bright field or in phase contrast modes using a Digital Optical Microscope DC3-163-PH with Integrated Imaging System (Microscope World, CA). The microscope was equipped with a charge-coupled device camera. Optical examination of the hydrogel macroparticles showed that their size varied between 1000 and 6000 mm. Optical examination of hydrogel microparticles showed[10] that in the shrunken state (pH 7.5), the major portion was significantly smaller than 160 μm in size and the maximum size never exceeded the membrane pore size. The maximum size of the swollen particles exceeded the size of the membrane pores at a pH of 4.5. Thus, despite nonspherical shape and significant polydispersity (20−200 μm), the specific surface area of microgels can be estimated to be of 50−100 times higher than that for macrogels.

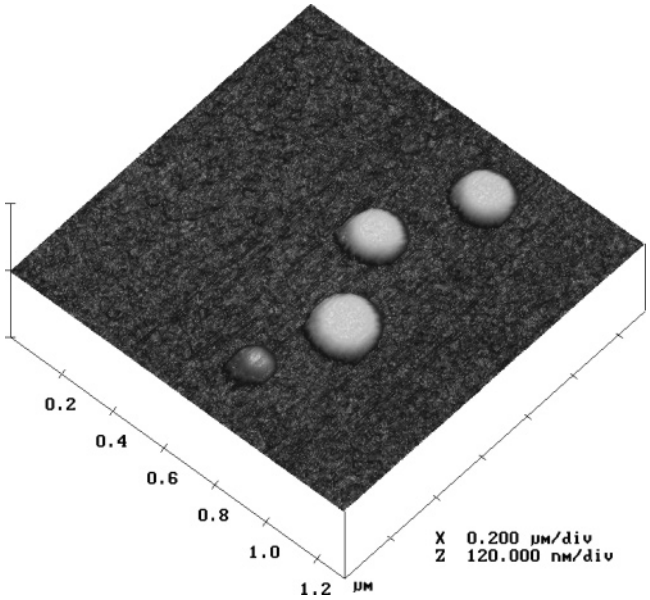

Figure 1. Tapping-mode 3D AFM image of PNIPA-VI nanogels amplitude data.

Nanogels Preparation. Nanometer-sized hydrogel particles (nanogels) were prepared by a modified method given elsewhere.[10,35] In brief, the interior to liposomes was used as a microreactor for polymerization. To prepare liposomes containing a pre-gel medium, a needed volume of EPC/chloroform solution with a phospholipid concentration of 20 mg/mL was poured into a round-bottom flask. To form a lipid film, the chloroform was evaporated under flushing with nitrogen. The film was held under vacuum for at least 3 h more and then hydrated by dispersing it in an aqueous solution of monomers (NIPA and VI), cross-linker (MBA), and photoinitiator (DEAP). The volume of a hydrogel-forming solution was chosen to provide the final concentration of 5 mg/mL EPC. After sonication of the suspension of multilamellar vesicles (MLV), the contents of the interior and exterior of the resultant large unilamellar vesicles (LUV) were identical. The suspension of LUV was diluted 25-fold with distilled water to prevent polymerization in the solution exterior to the liposomes. Further UV exposure of the solution initiated free radical polymerization, leading to gelation within the liposomal reactor. The hydrogel particle resides within the spherical phospholipid bilayer. To obtain bare hydrogel particles, the phospholipid was removed with 15 mM Triton X-100. The formed phospholipid/detergent micelles were removed by dialysis in SpectraPore 50 kDa membrane bags against water for 7 days with changing water twice a day. The atomic force microscopy (AFM) image of the synthesized nanogels is shown in Figure 1.

AFM. The AFM measurements were carried out in the tapping mode in free air with a Multimode NanoScope IIIa (Digital

Instruments, Santa Barbara, CA). Nanogels (4 μL) dispersion was deposited on fresh mica cleaved by pressing adhesive tape against the top mica surface and peeling off the tape. The sample was dried under the nitrogen flow. The studies were performed without preincubation outside the microscope. Software analysis was used on- and offline to provide the quality of recorded images. All measurements were done at room temperature (25 °C).

Dynamic Light Scattering (DLS). The size of obtained hydrogel nanoparticles was examined by the DLS technique using a N4 Plus particle size analyzer (Beckman-Coulter, Fullerton, CA) utilizing a 10-mW He−Ne laser as a light source. The temperature was stabilized at 25 ± 0.1 °C. The measurements were carried out at the constant scattering angle of 90°. Suspensions of nanogels were filtered into a square glass cuvette (10 mm) using a 0.45 μm Millipore Millex filter. The quality of measurements was checked over the apparent signal-to-noise ratio of the autocorrelation function, the overflow count, and the baseline error. When the field−field correlation function was close to single exponential, the cumulant analysis was used. The particle size distribution and the average particle diameter were obtained from the correlation function using the standard software provided by Beckman-Coulter.

In general, integral scattering intensity is a complex function of the concentration and size of particles fluctuations and the difference in refractive indices for the particles and solvent.[36,37] The DLS technique gives the information on the diffusion coefficient of the moving particles. The so-called average hydrodynamic diameter, $\langle d_h \rangle$, for the particles can be extracted from the DLS data using the well-known Stokes−Einstein relationship defining the size of a hydrodynamically effective sphere

$$\langle d_h \rangle = k_b T / 3\pi\eta D \quad (1)$$

where D is the diffusion coefficient, η is the solvent viscosity, T is the absolute temperature, and k_b is the Boltzmann's constant. All nanogel preparations had a unimodal size distribution where the average size varied from 30 to 300 nm at pH 7.5 and 25 °C.

Thus, there were two types of hydrogels prepared: one sensitive to pH (PNIPA-VI) and another that was not (PNIPA). Vinyl imidazole provides the pH-sensitive groups on polymeric chains of the hydrogel. Three types of hydrogel particles were prepared: macrogel (1000−6000 μm), microgel (~20−200 μm), and nanogel (~0.2 μm). The particles were suspended in a needed volume of water. The AFM- and DLS-characterized suspensions of hydrogel particles were used for swelling/shrinking measurements, potentiometric titration, and time-resolved pH measurements.

Potentiometric Titration of Pure Water, Microgel Particles, and Nanogels. An adjustment of pH by addition of HCl or NaOH changes the electrolyte concentrations and makes it difficult to discriminate between the pH and salt effect. To minimize the salt effect, both pure distilled water and aqueous suspension of hydrogel with pH 5.75 and 7.85, respectively, were taken as starting points for potentiometric titration toward acidic or basic ranges. The samples were stirred at ~70 rpm during titration. To confirm reproducibility, two different pH meters were used. A Hanna Checker 2 pH-meter (Hanna Instruments Inc.) was equipped with a combination pH electrode (model HI 1207). A MI-4154 microcombination electrode (Microelectrodes inc., Bedford, NH) with the response time of 5 s was interfaced to the computer. Vernier Logger Pro (v2.3) software was used for data acquisition, analysis, and storage. Both electrodes were calibrated by using three IUPAC standard buffers at pH 4, 7, and 10. All measurements were performed at 25 °C.

Time-Resolved pH Measurements. The apparatus described elsewhere[38] was used for real-time measurements of pH and simultaneous recording of the light transmitted through the cuvette. Briefly, the apparatus consists of a thermostated 1-mL cuvette assembled with a horizontally oriented pH electrode (Radiometer, type K4112), Ag/AgCl reference electrode, light-emitting diode as a light source (λ = 630 nm), and photodetector. There was no information from the manufacturer on the response time of the pH electrode used, so that the measurements carried out with the apparatus should be considered as qualitative. The configuration of the apparatus provides (1) simultaneous detection of the pH and the intensity of light passing through the cuvette and (2) injection of acid or base into the inner volume without electrode perturbations. As a matter of fact, swelling of hydrogel particles causes an increase in light transmission due to a decrease in the particle density, whereas shrinking results in a decrease in the transmitted light. The electrodes were interfaced with PC through a preamplifier and a commercially available A/D converter (12-bit, 70 kHz maximal sample rate). The original software provided real-time data acquisition, analysis, and storage. Water (1.0 mL) was poured into the cuvette. pH was equilibrated upon stirring and measured along with the intensity of light transmitted through the sample. After 30 s of recording, acid or base was injected into the cuvette through the hole in the cap. The measurements were carried out with a sample time of 0.1 s.

The quantitative kinetic measurements were carried out as follows: (1) a MI-4154 micro-combination electrode was calibrated, (2) 1.0 mL of pure water or 10 wt % of hydrogel suspension was placed in a well, (3) the sample was stirred with a stirring rod (1.5 × 2 × 5 mm) at ~70 rpm during measurements, (4) pH was equilibrated upon stirring for 30−100 s of recording the signals, (5) then acid was injected into the cuvette under permanent signal recording continued for the next 20−40 min with a sample time of 0.1 s. The measurements were performed at room temperature (~23 °C).

Results and Discussion

Swelling/Shrinking of Microgel Particles. The prepared microparticles (1000 mg) were suspended in 19 mL of distilled water within cylindrical vials. The suspension in each vial was sonicated for 10 min, and then the microgel particles were left at room temperature to precipitate and form a milky cylinder (the method of "precipitated cylinders"). After the equilibrium was reached (~2 h), pH was adjusted, and the cylinder heights were compared at four pHs. The cylinders with the equal weight amount of (a) PNIPA-VI and (b) PNIPA microgel particles were photographed at different pHs (Figure 2).

In Figure 2a, the ion sensitivity of the PNIPA-VI hydrogel containing the ionizable imidazolyl groups is demonstrated as a pH dependence of the microgel volume. In the range of pH from 10 to 6.8, the height of the milky cylinder is small and slightly increases with decreasing pH. In this range, the polymer network is in a collapsed state because the portion of neutral imidazolyl groups is still high. The conversion of the ionizable groups into the protonated form can result in the polymer network swelling due to imbalance between repulsive electrostatic forces and attractive elastic forces of the polymer network. This trend is more substantial when pH decreases from 6.8 to 4.5. If the concentration of acid ions (H^+ and Cl^-) elevates in the solvent surrounding gel particles, those ions are attracted into the gel and involved in the protonation of imidazolyl groups. Until all ionizable groups are protonated, a decrease in pH increases the electrostatic repulsion between polymer chains. To compensate it, the polymer network swells drastically.

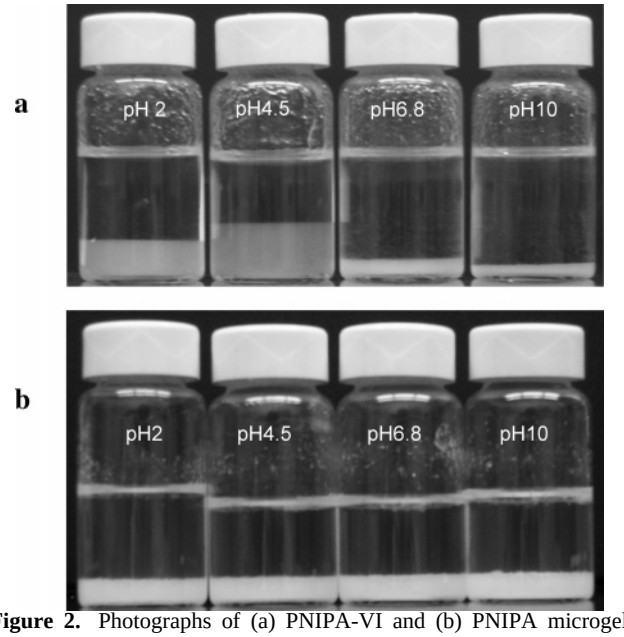

Figure 2. Photographs of (a) PNIPA-VI and (b) PNIPA microgel aqueous suspensions at different pH. Each vial contains equal weight amount of hydrogel.

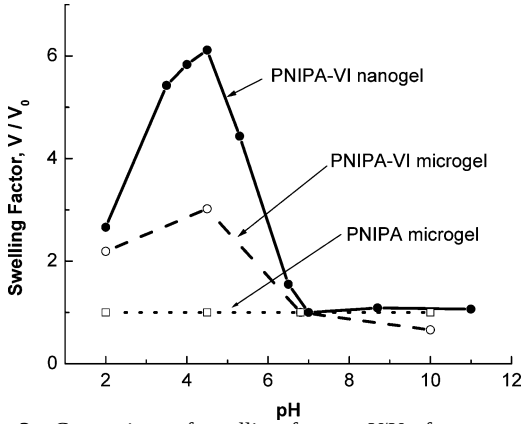

Figure 3. Comparison of swelling factors, V/V_0, for nanogels and microgels. V_0 is the volume of hydrogels at pH 7. The swelling factors for nanogels and microgels were calculated from the DLS data and Figure 2, respectively.

Eventually, all imidazolyl groups will be converted into the saline form at pH 4.5.

At a pH of less than 4.5, the excess of acid ions (H^+ and Cl^-) in the vicinity of the ionizable groups in the gel will result in their screening.[39,40] The latter phenomenon leads to a drop in the ion swelling pressure and microgel contraction which was observed in the pH range from 4.5 to 2.

On the contrary, Figure 2b illustrates that the volume of PNIPA microgels without ionizable groups is not pH sensitive: the height of the milky cylinders in all vials is the same in the whole range of pH studied.

Effect of pH on Size of PNIPA-VI Nanogels. Hydrogel nanoparticles composed of PNIPA network with the cationic monomer, VI, incorporated by UV-induced polymerization, exhibit both temperature and ionic sensitivity as reported in ref 35. But here we focus on pH sensitivity of the nanogels. The size of the hydrogel nanoparticles was analyzed at different pHs by DLS. The pH-dependence of the volume for PNIPA-VI nanogels was presented as the swelling factor in Figure 3. The data demonstrate the increase in the diameter $\langle d_h \rangle$ from 75 nm at pH 6.5 to 128 nm at pH 4.5 when the neutral imidazolyl groups become protonated. At pH < 4.5, the screening of protonated imidazolyl groups by an excess of acid ions results in gel contraction. On the contrary, there is no significant change in size of hydrogel nanoparticles upon pH increase from 7 to 11 by NaOH addition.

The swelling factors of nanogels obtained from the DLS data were compared to those for PNIPA-VI and PNIPA microgels extracted from Figure 2. Although the general tendency of swelling/shrinking with pH is the same for ion-sensitive nanogels and microgels (PNIPA-VI), the results demonstrate that the extent of swelling/deswelling for microgels is remarkably less than for nanogels. This fact presumably can be assigned to the heterogeneity of the microgels in terms of both particle size and density of polymer network. Roughly speaking, in larger hydrogel particles, the average extent of swelling/deswelling may be incomplete and equilibration of the particle dimensions takes a substantially longer time compared to the nanoparticles. PNIPA microgels exhibit the same volume for every pH reflecting their ionic insensitivity.

Potentiometric Curve for PNIPA-VI Microgels. Figure 4a shows pH-titration curves of 8.33 vol % PNIPA-VI microgel suspension (1) and pure water (2). We assumed that the addition of H^+ or OH^- into the suspension of a pH-sensitive microgel would change first the pH value of the external solution so that it would correspond to that for pure water. Indeed, this was observed. But afterward, the pH of the external solution was changed in accord with the proton flux direction as depicted by up and down arrows in Figure 4a. The difference in the

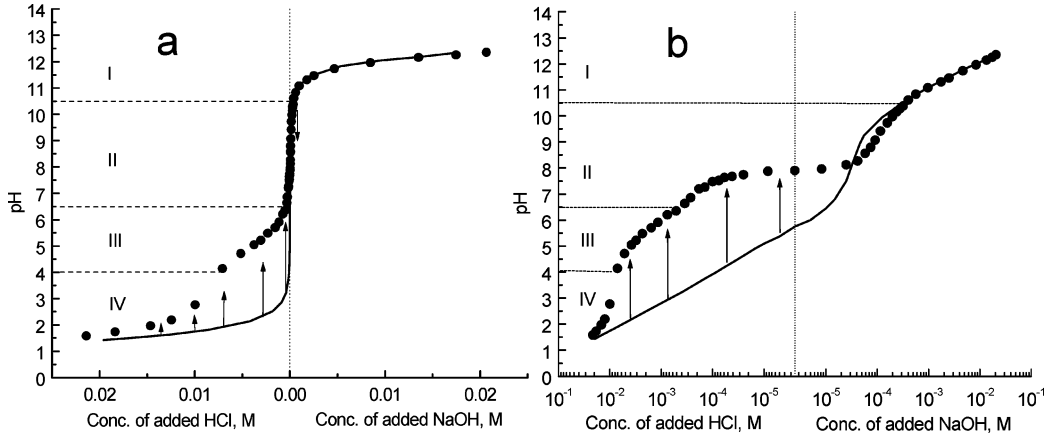

Figure 4. Changes in pH during titration of pure water (solid curve) and suspension of 8.33 vol % PNIPA-VI microgel (closed circles) with 0.1 M HCl and 0.1 M NaOH. (a) *X* axis in linear scale, (b) *X* axis in logarithmic scale. Arrows show the direction of pH equilibration after HCl or NaOH addition.

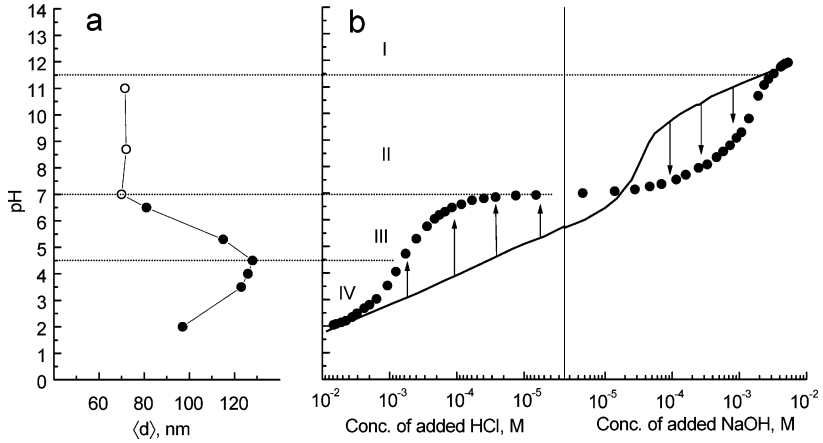

Figure 5. (a) pH dependence of the average diameter of pure PNIPA-VI nanogels. pH was decreased by addition of 0.1 M HCl (solid circles) and increased by addition of 0.2 M NaOH (open circles). (b) Changes in pH during titration of pure water (solid curve) and PNIPA-VI nanogels suspension (closed circles). Arrows show the direction of pH equilibration after HCl or NaOH addition.

measured external pH values for hydrogel suspension and pure water represents the ion capacity of a hydrogel ionic reservoir.

Figure 4a shows the most significant difference between a microgel suspension and pure water at pH values lower than 6.5, with the maximum at pH ≈ 4.5. At pH < 2, the solution pH leads toward pH of pure water. In the range of pH between 6.5 and 10.5, the titration curves for microgel suspension and pure water are indistinguishable in the linear scale used in Figure 4a. However, the difference between the titration curves can be visualized if the curves are plotted in logarithmic scale (Figure 4b). Unexpectedly, there is a significant difference between pure water and microgel suspension at pH > 7, where microgel exhibits only minor changes in the volume (see Figures 2 and 3).

Potentiometric Curve for PNIPA-VI Nanogels. The pH titration curve for PNIPA-VI nanogel aqueous suspension in comparison to that for pure water is presented in Figure 5b. The shape of the titration curve is explained by accumulation of acid ions inside the gel in acidic medium and their release in basic medium. The titration curve for nanogels exhibits a more significant deflection from the titration curve for water in the pH range from 7 to 11.5, as compared to microgels. According to Figure 5a, the nanogels do not substantially change the size in this pH range.

Since the penetration of ions through the gel/water surface is governed by restricted diffusion, one can expect that the total amount of ions accumulated in/released from gel should depend on the physical dimensions of the gel particles. The difference between titration curves for nanogels and water is more pronounced than that for microgels and water (see Figures 4a and 5b). For the same reason, the difference between titration curves of nanogels and water is still observed in the pH range of 2−6.5, despite the 8-fold lower concentration of nanogels than that of microgels. These results point out that diffusion of ions inside/outside the gel and their binding to ionizable groups along the polymer network occurs with a higher efficiency for hydrogel particles of a smaller size. In other words, the lesser is the size of hydrogel particles, the larger is the hydrogel volume involved into the process of ion accumulation/release, especially at the very beginning.

Four pH regions can be distinguished in the hydrogel ionic reservoir:

(I) pH > 11.5, almost all imidazolyl groups are deprotonated and hydrogel suspension behaves like pure water;

(II) 11.5 > pH > 7, hydrogel accumulates H^+ and Cl^- ions without significant change in volume;

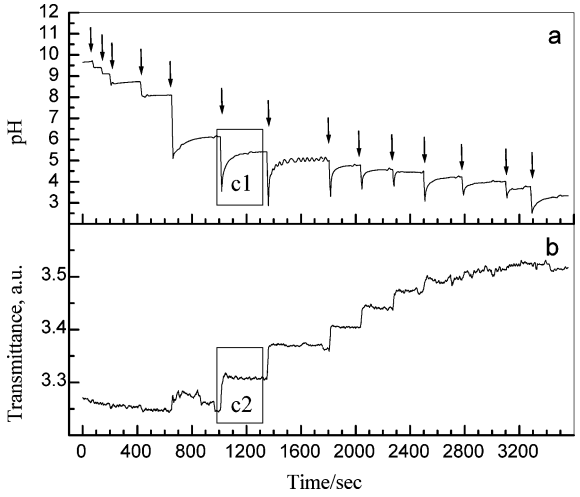

Figure 6. Time course of the external pH (a) and light transmittance (b) changes after a series of HCl injections into the suspension of 8% PNIPA-VI macrogel. Panels c1 and c2 correspond to the external pH and light transmittance changes, respectively, after the sixth injection (see the text).

(III) 7 > pH > 4.5, ions couple with ionizable groups on polymer network resulting in pronounced swelling;

(IV) pH < 4.5, screening of ionizable groups results in a decrease of the extent of swelling till all protonated groups are screened, and hydrogel suspension behaves again as pure water.

Qualitative Time-Resolved pH Measurements. A two-step mechanism can be proposed to describe the changes in the proton concentration in the solution external to hydrogel particles: first, fast binding of ions to immediate surface of each particle, and second, a successive diffusion of bound ions into the next inner layer of polymer network; herein, the ions from exterior will bind the newly vacant sites on the particle surface. Both steps represent one and the same process, i.e., ions' binding to the ionizable groups. This assumption was tested qualitatively for macro- and microgels. The other goal of the qualitative measurements was to demonstrate the ability of commercially available pH electrodes to resolve the time course of pH changes in the external solution in the presence of hydrogel.

PNIPA-VI Macrogels. The suspension of macrogel (8 vol %) with an approximate average size of ∼1 mm was tested by simultaneous recording pH (Figure 6a) and light transmission (Figure 6b). A series of HCl injections was done to change pH from 10 to 2. The first four injections of HCl decreased pH from 10 to 8 (Figure 6a), but the transmitted light changed

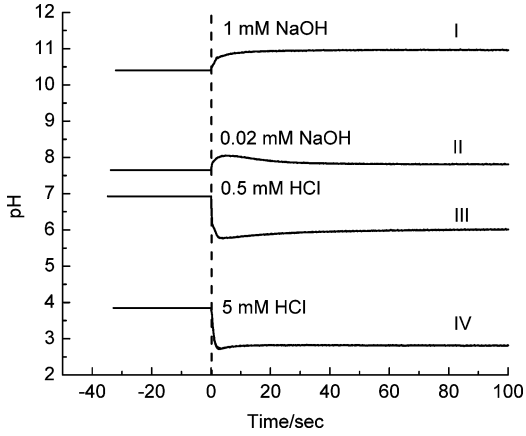

Figure 7. The time course of pH changes induced by HCl or NaOH injections (arrows) into the PNIPA-VI microgel suspension (8.3 vol %) depending on the region (roman numbers) corresponding to Figure 5.

negligibly indicating the absence of swelling (Figure 6b). The next injection decreased the external pH down to 5, at which hydrogel showed the first "pulse" of swelling (Figure 6b). Immediately after that, the pH of the external solution began to increase and reached the plateau corresponding to a lesser swelling degree. In the course of the sixth injection, pH passed through the maximum of swelling at pH 4.5 and reached the interval where hydrogel shrunk as a result of polymer network charge screening (see panel c1 in Figure 6a). Thus, the final pH corresponds to the swollen state of hydrogel but not to the maximum swelling. That is why the average level of light transmittance (see panel c2 in Figure 6b) decreases exponentially showing the further minor hydrogel shrinking, whereas some oscillations of light transmittance occur in the transitional interval starting in ~50 s after injection.

Further injections show (Figure 6b) that swelling of hydrogel stops and hydrogel begins to shrink, when the equilibrium pH becomes lower than 4 (Figure 6a).

PNIPA-VI Microgels. Time-dependent measurements were performed with four samples of microgel suspended in pure water, with the initial pH values of ca. 10.4 (I), 7.6 (II), 6.9 (III), and 3.8 (IV). According to the titration curve (Figure 4), the microgel suspension has different sensitivity to the concentration of added acid or base. This was the reason why different amounts of HCl and NaOH solution were injected into the samples. Four curves corresponding to four pH regions are presented in Figure 7. At the moment of base/acid injection, the pH increases or decreases rapidly. This process takes less than 2 s. The further process is significantly slower: equilibrium pH is reached in about 80 s.

It was interesting to compare the kinetics of ion exchange in microgels with their ability to swell for the first moment after the base or acid injection (Figure 8). The portion of light transmitted through the sample (or portion of scattered light) should depend on the difference between the refractive indices of hydrogel and water. As can be seen in Figure 2a, swelling decreases, whereas shrinking increases, this diference. Thus, an increase in the relative intensity of light transmitted through the microgel suspension was assigned to the swelling of hydrogel particles, whereas a decrease in the transmitted intensity corresponds to their shrinking.

In region I (initial pH 10.4, Figure 8a) no swelling/shrinking is detected as judged from curve 2, because the most imidazolyl groups inside hydrogel are deprotonated. A relatively slow increase in pH is observed (curve 1).

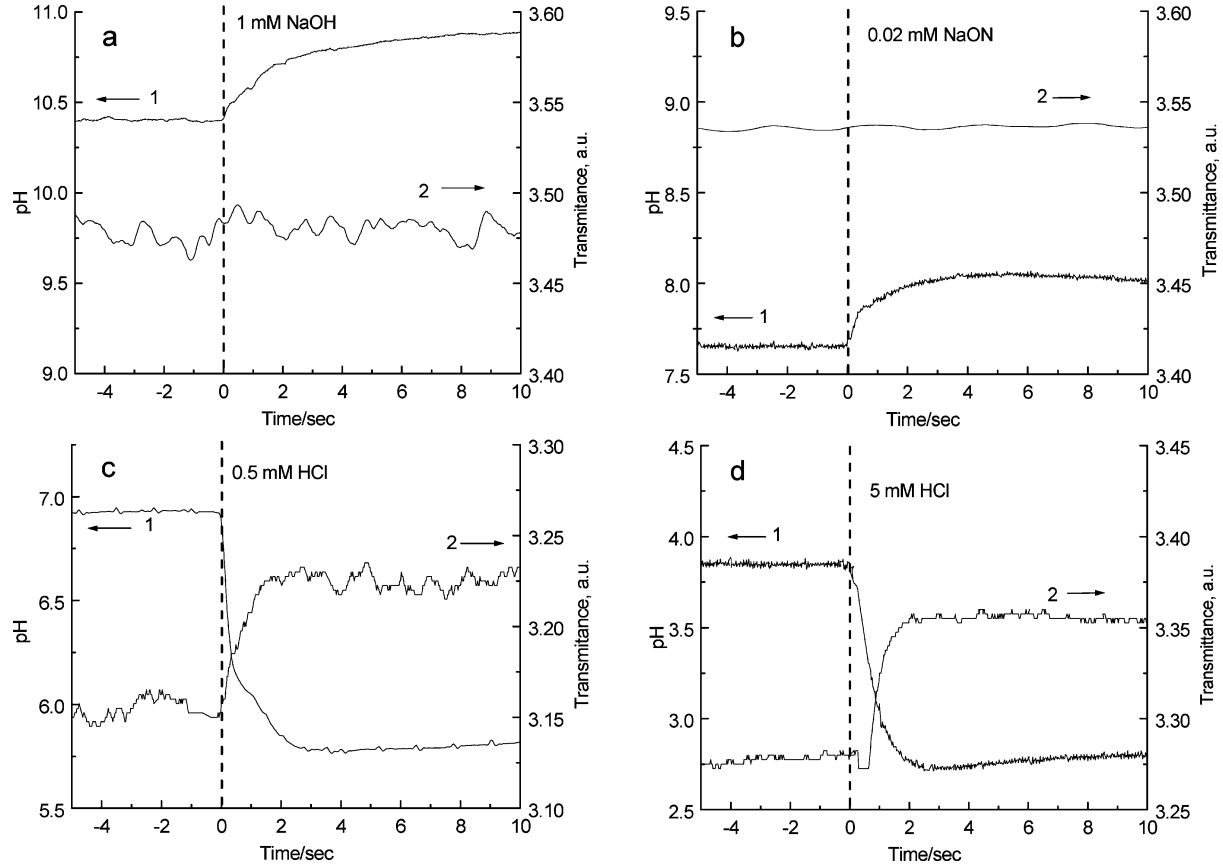

Figure 8. The time course of changes in pH (curve 1) and transmitted light intensity (curve 2) induced by NaOH (a, b) and HCl (c, d) injections (dashed vertical lines) into the PNIPA-VI microgel suspension (8.3 vol %) at initial pH values of 10.4 (a), 7.6 (b), 6.9 (c), and 3.8 (d).

In region II (initial pH 7.6, Figure 8b) no swelling/shrinking is detected (curve 2). Curve 1 shows that the flux of H^+ ions from the interior to exterior of hydrogel compensates the hydroxyl ions in half a second after NaOH injection; in 4−5 s after the injection, this flux begins to decrease the pH in external solution. In contrast to the previous case, a portion of protonated imidazolyl groups inside hydrogel is significant and can release protons to the gel exterior.

For the initial pH 6.9 (Figure 8c, region III), the addition of 0.5 mM HCl results in the transmittance increase, indicating microgel swelling (curve 2). Curve 1 shows that pH decreases to 6.2 in 0.5 s after HCl injection. The initiated gel swelling slows down the rate of pH changes. The pH minimum achieved in 3 s after acid injection is followed by slow increase in pH.

At the initial pH < 4 (Figure 8d, region IV), the addition of 5 mM HCl results in microgel swelling (curve 2): the transmittance reaches the maximum and then slowly decreases indicating some screening of the ionizable groups. Because of microgel swelling, the drop in pH is slower than that for region III and lasts 3 s after the acid injection (curve 1). The following increase in pH is less pronounced than for region III, because the majority of ionizable sites has been already protonated at these pHs.

The fact that transmittance rises just after the acid injection at pH < 4 while the screening effect develops much later, allows us to assume that microgels are somewhat heterogeneous in terms of both particle size and polymer network density. Roughly speaking, for large hydrogel particles, ion diffusion through the hydrogel/water boundary is hampered and, therefore, the average extent of swelling/deswelling is not complete if compared to nanoparticles. This point is supported by the pH-dependence of hydrogel size presented in Figure 3.

Quantitative Time-Resolved pH Measurements for Hydrogels of Different Size. To reveal quantitative, or at least semiquantitative, parameters that may characterize size-dependent kinetics of proton binding, the kinetics of proton consumption by macro-, micro-, and nanogels after acid addition has been thoroughly compared with pure water under the same experimental conditions. For these measurements, a microelectrode (MI-4154 micro-combination electrode from Microelectrodes Inc., Bedford, NH) with the known response time (5 s) was used.

As shown in Figure 9a, pH-equilibration time course for PNIPA-VI hydrogels is qualitatively similar for all particle sizes (1, 2, 3): pH sharply drops toward that of pure water (4), and then pH begins to rise and finally reaches a plateau. Obviously, if the concentration of ionizable groups inside polymer network is much higher than the concentration of protons added, the equilibrium pH will be close to the initial one. The time to reach the equilibrium plateau differs strikingly for macro-, micro-, and nanogels: the bigger the particles, the longer the time. Moreover, the bigger are the particles, the deeper is the drop in pH after acid addition into the suspensions under the same experimental conditions. Minor changes in the time course of pH-equilibration for pure water after acid addition (4) may be an "instrumental" effect due to the ion leakage through the microelectrode surface.

Figure 9b shows that the time course of pH-equilibration for PNIPA hydrogel particles which contain no ionizable groups is similar to that of pure water. The comparison of PNIPA-VI and PNIPA pH-equilibration kinetics (parts a and b of Figure 9) proves that the kinetics of proton binding to the imidazolyl groups on the polymer network is size dependent.

To visualize the difference between the time courses of pH equilibration in the hydrogel suspensions of different size, the data in Figure 9a were replotted in logarithmic scale (Figure 10). Herein, pH was recalculated into the proton concentration $[H^+]$ and also represented in log scale. Now, in the log−log scale, the peculiarities of proton binding by hydrogels in the initial period can be clearly seen (Figure 10).

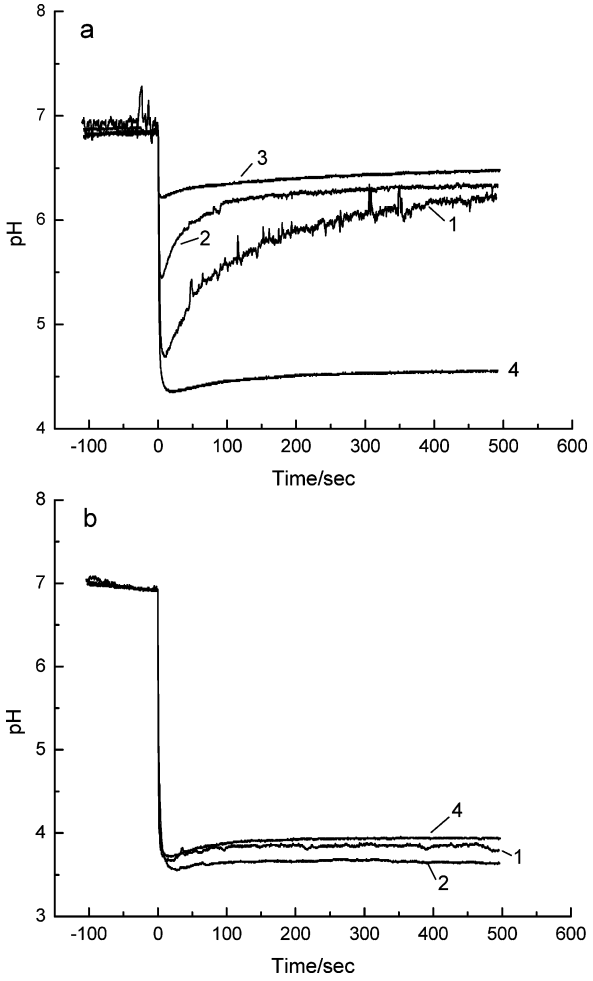

Figure 9. The time course of pH after addition of 5 μL of 0.1 M HCl into 1.2 mL of (a) PNIPA-VI or (b) PNIPA (1) macrogels, (2) microgels, and (3) nanogels suspensions or (4) pure water.

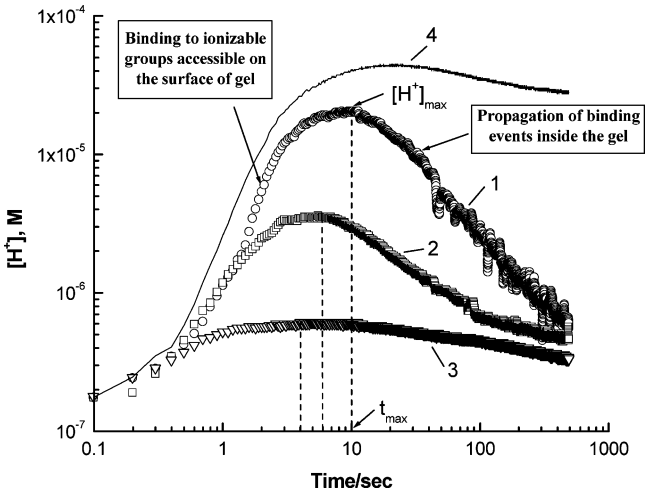

Figure 10. log−log presentation ($\log[H^+] = f[\log(t)]$) of the time course of proton concentration $[H^+]$ after addition of 5 μL of 0.1 M HCl into 1.2 mL of PNIPA-VI (1) macrogels, (2) microgels, (3) nanogels suspensions, and water (4).

The distinct behavior of the three curves from the first second indicates different rates of proton suction: the slope increases with the particles size. Both the magnitude of $[H^+]$ maximum

TABLE 1: Kinetic Parameters of Proton Consumption by PNIPA-VI Hydrogel of Different Sizes

gel	size, μm	[X + A*], 10^{-5} M	A_1, 10^{-5} M	τ_1, s	A_2, 10^{-5} M	τ_2, s
macro	1000−6000	2.7	3.9	12.7	−1.2	128
micro	20−200	2.8	4.7	5.8	−1.9	102
nano	∼0.2	2.8	4.8	5.2	−2.0	98

and its location on a time scale are in phase with the size of hydrogel particles: the bigger are the particles, the higher is the maximum ($[H^+]_{max}$) and the longer is the time period to the maximum (t_{max}) (Figure 10).

This observation can be assigned to the difference in the specific surface areas for particles of different sizes: the smaller is the gel, the higher is the total surface area, and therefore, the larger number of ionizable groups is available for proton binding. For nanogels, the added protons bind to those ionizable groups very rapidly resulting in an abrupt decrease in the $[H^+]$ gradient between interior and exterior to hydrogels, so that the rate is slower and $[H^+]$ maximum is lower than for micro- and especially macrogels. The existence of $[H^+]$ maximum results from competition between diffusion of added protons into the volume of the sample and proton binding on the hydrogel surface. The propagation of the binding "wave" toward the center of the gel particle dominates once the maximum concentration is reached.

Quasichemical Kinetic Model. To describe pH equilibration shown in Figure 10 quantitatively, a kinetic model of relaxation to equilibrium was applied. There are three types of protons in the system: A is an injected proton, X is a proton bound to the surface site (intermediate compound), and A* is a proton bound in the bulk of hydrogel. The following reversible reactions describe the system after acid addition

$$A \underset{k_{-1}}{\overset{k_1}{\rightleftharpoons}} X \underset{k_{-2}}{\overset{k_2}{\rightleftharpoons}} A^* \qquad (2)$$

where k_1 and k_2 are rate constants for forward reactions and k_{-1} and k_{-2} are rate constants for reverse reactions. The system of three differential equations and equation of material balance describes reaction 2

$$(d[A]/dt) = -k_1[A] + k_{-1}[X]$$

$$(d[X]/dt) = k_1[A] - (k_{-1} + k_2)[X] + k_{-2}[A^*] \qquad (3)$$

$$(d[A^*]/dt) = k_2[X] - k_2[A^*]$$

$$[A_0] = [A] + [X] + [A^*] \qquad (3a)$$

where $[A_0]$ is the concentration of protons (acid) initially injected into the hydrogel suspension. At the boundary conditions

$$[A]_{t=0} = [A_0];\ [X]_{t=0} = 0;\ [A^*]_{t=0} = 0;\ [A]_{t=\infty} = [A\infty];\ [X]_{t=\infty} = [A^*]_{t=\infty} \qquad (4)$$

System (3) has the analytical solution in the form

$$[A] = [A]\infty + A_1 e^{-t/\tau_1} + A_2 e^{-t/\tau_2} \qquad (5)$$

where τ_1 and τ_2 are the characteristic times of the processes, which can be presented as functions of the corresponding rate constants

$$-(1/\tau_{1,2}) = -(k_1 + k_{-1} + k_2 + k_{-2}/2) \pm \sqrt{((k_1 + k_{-1} + k_2 + k_{-2})^2/4) - (k_1k_{-1} + k_1k_2 + k_1k_{-2} + k_{-1}k_{-2})} \qquad (6)$$

Values of τ_1 and τ_2 can be found from any experimental data {[A](t), [X](t), or [A*](t)}. In our experiment, the concentration of protons in exterior to hydrogel particles, [A], was measured. However, as seen in Figure 10, these measurements can be perturbed by the electrode leakage (cf. curve 4 for the pH time course in pure water). To minimize this "instrumental" effect, the total concentration of protons bound inside the gel, [X + A*], was determined by the subtraction of the measured proton concentrations in water $[H^+]_{water}$ and hydrogel suspension $[H^+]_{HG+water}$ at each time (eq 7). The resultant curves are presented in Figure 11.

Taking into account the equation of material balance (eq 3a) and the system solution (eq 5), the curves in Figure 11 should be described by the following expression

$$\Delta[H^+] = [H^+]_{water} - [H^+]_{HG+water} = [A]_0 - [A] = [X + A^*] = [A]_0 - [A]_\infty - A_1 e^{-t/\tau_1} - A_2 e^{-t/\tau_2} \qquad (7)$$

From the boundary conditions (eq 4) one can obtain the following relationships between the coefficients: $[A]_0 - [A]_\infty = A_1 + A_2$, leading to the final two-exponential equation which was used for fitting the data in Figure 11

$$\Delta[H^+] = [X + A^*] = A_1(1 - e^{-t/\tau_1}) + A_2(1 - e^{-t/\tau_2}) \qquad (8)$$

The squared regression factor R^2 ranged from 0.98 to 0.99 for all curves fitted in eq 8. The fitting parameters for macro-, micro-, and nanogels are summarized in Table 1.

All the parameters in Table 1 are size dependent. However, the insignificant extent of changes in the time characteristics (τ_1 and τ_2) in comparison to the extent of particle size variations was unexpected. Indeed, the time constant τ_2 increases ∼1.3 times from nanogels to macrogels, whereas the size changes by about 4 orders of magnitude. Certainly, the process of binding to the ionizable groups accessible on the surface of particles should be more substantially size dependent. The data indicate that binding processes for the micro- and nanogels are too rapid to be resolved by a microelectrode with the response time of ∼5 s. One can conclude that the time constant for this surface

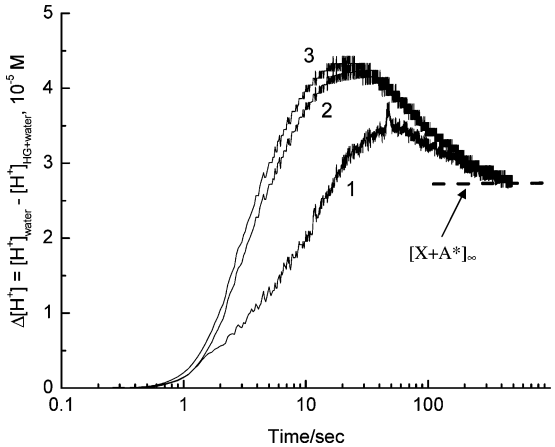

Figure 11. The time course of the concentration of protons bound inside the gel after addition of 5 μL of 0.1 M HCl into 1.2 mL of hydrogel suspension for (1) macrogels, (2) microgels, and (3) nanogels suspensions.

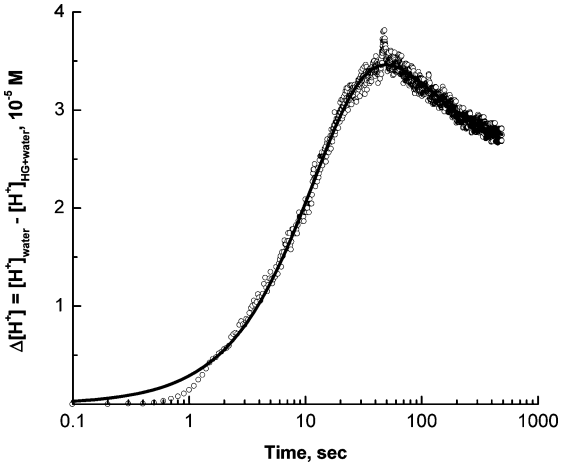

Figure 12. Fitting curve (solid line) with parameters from Table 1 for the time course of the concentration of protons bound inside the gel (open circles) after addition of 5 μL of 0.1 M HCl into 1.2 mL of PNIPA-VI macrogel suspension.

binding is significantly less than 5 s for both micro- and nanogels. The time constant τ_1 for macrogels is greater than the response time of the microelectrode. However, even in this case, the biggest deviation of the fitting curve from experimental data occurs at times less 5 s (Figure 12). Thus, the mechanism of proton consumption by hydrogel particles comprises at least two processes with distinct characteristic times, although the fast process within the initial 10 s cannot be distinguished by the inertial electrode.

Conclusions

This investigation was undertaken to describe mechanistic details of proton transport in and out of hydrogel particles of different sizes. The hydrogel particles of three different ranges were prepared: macrogel (1000−6000 μm), microgel (~20−200 μm), and nanogel (~0.2 μm). Two types of hydrogels were studied, i.e., sensitive (PNIPA-VI) and insensitive (PNIPA) to pH. A number of important conclusions were derived:

(1) There are three processes that effect on the solute transfer through the hydrogel/water boundaries, namely, swelling/deswelling of the hydrogel particles, accumulation of ions within gel matrix and their release to exterior, and binding or releasing ions by ionizable groups along the polymer network.

(2) Accumulation of ions within gel matrix and their release to exterior can occur without significant swelling/shrinking of hydrogel.

(3) The extent of swelling/deswelling for hydrogel particles as well as the efficiency of ion exchange between hydrogel ionic reservoir and external solution are both size- and homogeneity-dependent. Herein, binding or releasing ions by ionizable groups along the polymer network looks like the main effectors on both the characteristic time of changes in the external ion concentration and the swelling/shrinking features.

The time-resolved measurements of pH external to the hydrogel particles of different size allowed us to distinguish two mechanisms underlying the kinetics of proton consumption: (1) fast binding of the ions to the ionizable groups exposed on the immediate surface of each particle and (2) slower successive diffusion of bound sites into the deeper layers of polymer network.

According to the developed quasichemical kinetic model, the time course of proton uptake into either macro-, micro-, or nanogels is analytically described by a two-exponential equation with characteristic times τ_1 and τ_2. All parameters extracted (Table 1) are found to be size dependent; however, the rate of initial binding to the surface ionizable groups for micro- and nanoparticles appeared to be too fast to be resolved by a microelectrode with the response time of ~5 s. However, the recent reports on ion-responsive electrodes with the response time less than 10^{-3} s[41] make the idea of measuring fast ion exchange in the vicinity of the single nanoparticle realistic. One can dispute that fluorescence methods are fast and sensitive to follow pH kinetics.[42] Nevertheless, the method developed in this work has a number of advantages: (i) it is robust, versatile, noninvasive, easy sampling, and does not spoil the sample, so that the sample is ready for further examination after the measurements. The latter point is extremely important if only a small or limited amount of sample is available.

It is worthwhile to highlight that the developed kinetic model will be useful for the other types of natural or artificial ionic reservoirs and multifunctional containers, namely: (i) the experimental method and analytical model are expected to be informative for characterization of artificial systems such as drug delivery vehicles, actuators, biosensors, and wet nanoelectronics; (ii) for natural multilayered structures (cytoplasm, cells, mitochondria, bacterial spores, etc.), the extracted binding rates can be ascribed to their structural elements. The approach is easily extended for the other ions (e.g., Na^+, K^+, and Ca^{2+}) by replacing with the suitable electrode. These stages are under development in our laboratory.

Acknowledgment. This work was financially supported in part by Polytechnic University and Pace University (Dyson College of Art and Sciences, Summer Research Grant, and Scholarly Research Fund).

References and Notes

(1) Kiser, P. F.; Wilson, G.; Needham, D. *Nature* **1998**, *394*, 459.
(2) Peppas, N. A. *Curr. Opin. Colloid Interface Sci.* **1997**, *2*, 531.
(3) Yoshida, R.; Ichijo, H.; Yamaguchi, T. *Macromol. Rapid Commun.* **1995**, *16*, 305.
(4) Yoshida, R.; Toshikazu, T.; Hisao, I. *J. Am. Chem. Soc.* **1996**, *118*, 5134.
(5) Tabata, O.; Hirasawa, H.; Aoki, S.; Yoshida, R.; Kokufuta, E. *Sens. Actuators A* **2002**, *95*, 234.
(6) Giannos, S. A.; Dinh, S. M.; Berner, B. *Macromol. Rapid Commun.* **1995**, *16*, 527.
(7) Brock, D.; Lee, W.; Segalman, D.; Witkowski, W. *J. Intelligent Mater. Sys. Struct.* **1994**, *5*, 764.
(8) Sackmann, E.; Tanaka, M. *TIBTECH* **2000**, *18*, 58.
(9) (a) Yuan, H.; Ottova, L. A.; Tien, H. T. *Mater. Sci. Eng. C* **1996**, *4*, 35. (b) Lu, X.; Ottova, L. A.; Tien, H. T. *Bioelectrochem. Bioenegetics* **1996**, *39*, 285. (c) Ottova, L. A.; Tien, H. T. *Bioelectrochem. Bioenegetics* **1997**, *42*, 141. (d) Ivnitski, D.; Wilkins, E.; Tien, H. T.; Ottova, L. A. *Electrochem. Commun.* **2000**, *2*, 457.
(10) Kazakov, S.; Kaholek, M.; Levon, K. *Proc. SPIE* **2002**, *4695*, 42.
(11) Pollack, G. H. *Cells, gels and the engines of life*; Ebner & Sons: Seattle, WA, 2000.
(12) Ohmine, I.; Tanaka, T. *J. Chem. Phys.* **1982**, *77*, 5725.
(13) Ricka, J.; Tanaka, T. *Macromolecules* **1985**, *18*, 83.
(14) Ricka, J.; Tanaka, T. *Macromolecules* **1984**, *17*, 2916.
(15) Tanaka, T.; Fillmore, D.; Sun, S. T.; Nishio, I.; Suislow, G.; Shah, A. *Phys. Rev. Lett.* **1980**, *45*, 1636.
(16) Rubinstein, M.; Colby, R. H.; Dobrynin, A. V.; Joanny, J.-F. *Macromolecules* **1996**, *29*, 398.
(17) Khokhlov, A. R.; Kramarenko, E. Yu. *Macromolecules* **1996**, *29*, 681.
(18) Fernandez-Nieves, A.; Fernandez-Barbero, A.; Vincent, B.; de las Nieves, F. J. *Macromolecules* **2000**, *33*, 2114.
(19) Shibayama, M.; Ikkai, F.; Inamoto, S.; Nomura, S. *J. Chem. Phys.* **1996**, *105*, 4358.
(20) Eichenbaum, G. M.; Kiser, P. F.; Simon, S. A.; Needham, D. *Macromolecules* **1998**, *31*, 5084.
(21) Eichenbaum, G. M.; Kiser, P. F.; Dobrynin, A. V.; Simon, S. A.; Needham, D. *Macromolecules* **1999**, *32*, 4867.
(22) Eichenbaum, G. M.; Kiser, P. F.; Shan, D.; Simon, S. A.; Needham, D. *Macromolecules* **1999**, *32*, 8996.

(23) Markland, P.; Zhang, Y.; Amidon, G. L.; Yang, V. C. *J. Biomed. Mater. Res.* **1999**, *47*, 595.
(24) Suzuki, H.; Wang, B.; Yoshida, R.; Kokufuta, E. *Langmuir* **1999**, *15*, 4283.
(25) Ito, S.; Ogawa, K.; Suzuki, H.; Wang, B.; Yoshida, R.; Kokufuta, E. *Langmuir* **1999**, *15*, 4289.
(26) Ogawa, Y.; Ogawa, K.; Wang, B.; Kokufuta, E. *Langmuir* **2001**, *17*, 2670.
(27) Jeon, C. H.; Makhaeva, E. E.; Khokhlov, A. R. *Macromol. Chem. Phys.* **1998**, *199*, 2665.
(28) Katchalsky, A.; Steinberg, I. Z.; Oplatka, A.; Kam, A. US Patent No. 3,321,908, 1967.
(29) Ogawa, K.; Nakayama, A.; Kokufuta E. *Langmuir* **2003**, *19*, 3178.
(30) Kaggwa, G. B.; Carey, M. J.; Such, C.; Saunders, B. R. *J. Colloid Interface Sci.* **2003**, *257*, 392.
(31) López-Leon, T.; Ortega-Vinuesa, J. L.; Bastos-Gonzalez, D.; Elai1ssari, A. *J. Phys. Chem. B* **2006**, *110*, 4629.
(32) Hoare, T.; Pelton, R. *Langmuir* **2004**, *20*, 2123.
(33) Saunders, B. R. *Langmuir* **2004**, *20*, 3925.
(34) Hoare, T.; Pelton, R. *Macromolecules* **2004**, *37*, 2544.
(35) (a) Kazakov, S.; Kaholek, M.; Teraoka, I.; Levon, K. *Macromolecules* **2002**, *35*, 1911. (b) Kazakov, S.; Kaholek, M.; Kudasheva, D.; Teraoka, I.; Cowman, K. M.; Levon, K. *Langmuir* **2003**, *19*, 8086.
(36) Berne, B. J.; Pecora, R. *Dynamic light scattering with applications to chemistry, biology and physics*; Willey-Interscience: New York, 1976.
(37) Kazakov, S. V.; Galaev, I. Yu.; Mattiasson, B. *Int. J. Thermophys.* **2002**, *23*, 161.
(38) Krasnikov, B. F.; Zorov, D. B.; Antonenko, Y. N.; Zaspa, A. A.; Kulikov, I. V.; Kristal, B. S.; Cooper, A. J.; Brown, A. M. *Biochim. Biophys. Acta* **2005**, *1708*, 375.
(39) Saunders, B. R.; Crowther, H. M.; Vincent, B. *Macromolecules* **1997**, *30*, 482.
(40) Zhou, S.; Chu, B. *J. Phys. Chem. B* **1998**, *102*, 1364.
(41) Mückenhoff, K.; Schreiber, S.; DeSantis, A.; Okada, Y.; Scheid, P. *J. Neurosci. Methods* **1994**, *51*, 147.
(42) Mallik, R.; Udgaonkar, J. K.; Krishnamoorthy, G. *Proc. Ind. Acad. Sci.* **2003**, *5*, 307.